# Hierarchical clustering of brain activity during human nonrapid eye movement sleep

Mélanie Boly[a,1], Vincent Perlbarg[b,1], Guillaume Marrelec[b], Manuel Schabus[a,2], Steven Laureys[a], Julien Doyon[c], Mélanie Pélégrini-Issac[b], Pierre Maquet[a,3], and Habib Benali[b]

[a]Cyclotron Research Centre, University of Liège, 4000 Liège, Belgium; [b]Institut National de la Santé et de la Recherche Médicale–Université Pierre et Marie Curie Paris 06, Unité Mixte de Recherche-S 678, Laboratoire d'Imagerie Fonctionnelle, 75634 Cedex 13 Paris, France; and [c]Functional Neuroimaging Unit, Montreal Geriatrics Institute, Montreal, QC, Canada H3W 1W5

Edited by Marcus E. Raichle, Washington University in St. Louis, St. Louis, MO, and approved February 13, 2012 (received for review July 19, 2011)

**Consciousness is reduced during nonrapid eye movement (NREM) sleep due to changes in brain function that are still poorly understood. Here, we tested the hypothesis that impaired consciousness during NREM sleep is associated with an increased modularity of brain activity. Cerebral connectivity was quantified in resting-state functional magnetic resonance imaging times series acquired in 13 healthy volunteers during wakefulness and NREM sleep. The analysis revealed a modification of the hierarchical organization of large-scale networks into smaller independent modules during NREM sleep, independently from EEG markers of the slow oscillation. Such modifications in brain connectivity, possibly driven by sleep ultraslow oscillations, could hinder the brain's ability to integrate information and account for decreased consciousness during NREM sleep.**

complexity | integration

During nonrapid eye movement (NREM) sleep, we are less aware of ourselves and our environment and, if we awaken, are less able to recollect any mental representation than during full-blown wakefulness (1). The mechanisms underpinning the reduction in conscious content during NREM sleep are still uncertain. Consciousness has been associated with the ability of a system to integrate information (2), which could be altered during NREM sleep. Here, in contrast to previous work (3, 4), we quantified changes in information integration from wakefulness to NREM sleep in large-scale brain networks and computed both their *total integration* and their degree of *functional clustering*. Functional clustering estimates how integration is hierarchically organized within and across the constituent parts of a system. It has been proposed as an empirically tractable measure for complexity of brain integration (5), which is considered a better estimate of the capacity to integrate information than total integration (6).

We assessed brain functional connectivity on functional MRI (fMRI) data, which reflect the slow dynamics of local field potentials rather than instantaneous neural activities (7). Data were collected in a single nocturnal session in 13 participants who maintained periods of steady NREM sleep. At awakening, none of the subjects could recall any mental conscious content since sleep onset. From this dataset, we extracted for each subject two subsets of consecutive volumes recorded, respectively, during wakefulness and NREM sleep. Six spatially independent patterns, which we refer to as *networks* (Fig. 1*A*), were identified at the group level on wakefulness data, using a data-driven method (independent component analysis). These networks [visual (VIS), motor (MOT), default mode (DM), dorsal attentional (dATT), executive control (EC), and salience (SAL)] were previously identified in many studies investigating resting-state fMRI correlations in the literature (8–10). Network composition was very similar in data obtained during NREM sleep compared with wakefulness, in terms of within-networks areas distribution and Euclidian distance between networks (*SI Results* and Fig. S1). The six networks consistently identified during wakefulness were used only to select regions of interest (ROIs) for further analyses. In total, 77 ROIs were selected around the local maxima of these networks (Table S1). To quantify the amount of functional interactions within and between these networks across vigilance states, we computed a hierarchical measure of integration between brain regions during both NREM sleep and wakefulness. First, an average ROI activity time course was extracted and an averaged correlation matrix was computed for each network on NREM sleep data. On the basis of the resulting similarity tree, each network was further parsed in anatomically and physiologically meaningful assemblies of bilateral homologous areas (Fig. S2). We then considered brain connectivity at three nested levels: brain, networks, and assemblies of areas (Fig. 1*B*). The brain was divided into six networks and each network into three to seven assemblies of two to five areas. Finally, we probed the hierarchical structure of brain integration by computing integration at whole-brain and network levels and derived their respective functional clustering ratio (FCR), the proportion of interactions within each subsystem, relative to between them. Differences in FCR between wakefulness and NREM were tested in a Bayesian framework and inferences were conducted at a probability of difference >0.95.

## Results

Compared with wakefulness, NREM sleep was characterized by a diffuse increase in FCR values, both at the whole-brain level and in each and every brain network (Fig. 1*C* and Table 1). Rather than the mere breakdown of functional connectivity (11), this result reveals a profound modification of the hierarchical organization of functional integration. Total brain integration increased during NREM sleep relative to wakefulness (Table 2) due to an increase in both within- and between-network integration. Within each network, a fairly consistent change consisted of an increase in within-assembly integration ($I_{ws}$), observed in all networks except the MOT network (Table 3). In contrast, during NREM sleep, the integration between assemblies ($I_{bs}$) increased (VIS and ATT), remained stable (EC), or decreased (MOT, DM, and SAL; Table 4). However, in all networks, the change in within-assembly integration was proportionally larger than that in between-assembly integration, resulting in a consistent increase in FCR. Complementary analyses revealed that this (fixed-effects) group result of an increase in FCR during NREM sleep compared with wakefulness was reproducible across indi-

Author contributions: M.S. and P.M. designed research; M.B. and M.S. performed research; V.P., G.M., and H.B. contributed new reagents/analytic tools; M.B., V.P., G.M., M.P.-I., P.M., and H.B. analyzed data; and M.B., V.P., G.M., S.L., J.D., M.P.-I., P.M., and H.B. wrote the paper.

The authors declare no conflict of interest.

This article is a PNAS Direct Submission.

[1]M.B. and V.P. contributed equally to this work.

[2]Present address: Department of Psychology, University of Salzburg, 5020 Salzburg, Austria.

[3]To whom correspondence should be addressed. E-mail: pmaquet@ulg.ac.be.

This article contains supporting information online at www.pnas.org/lookup/suppl/doi:10.1073/pnas.1111133109/-/DCSupplemental.

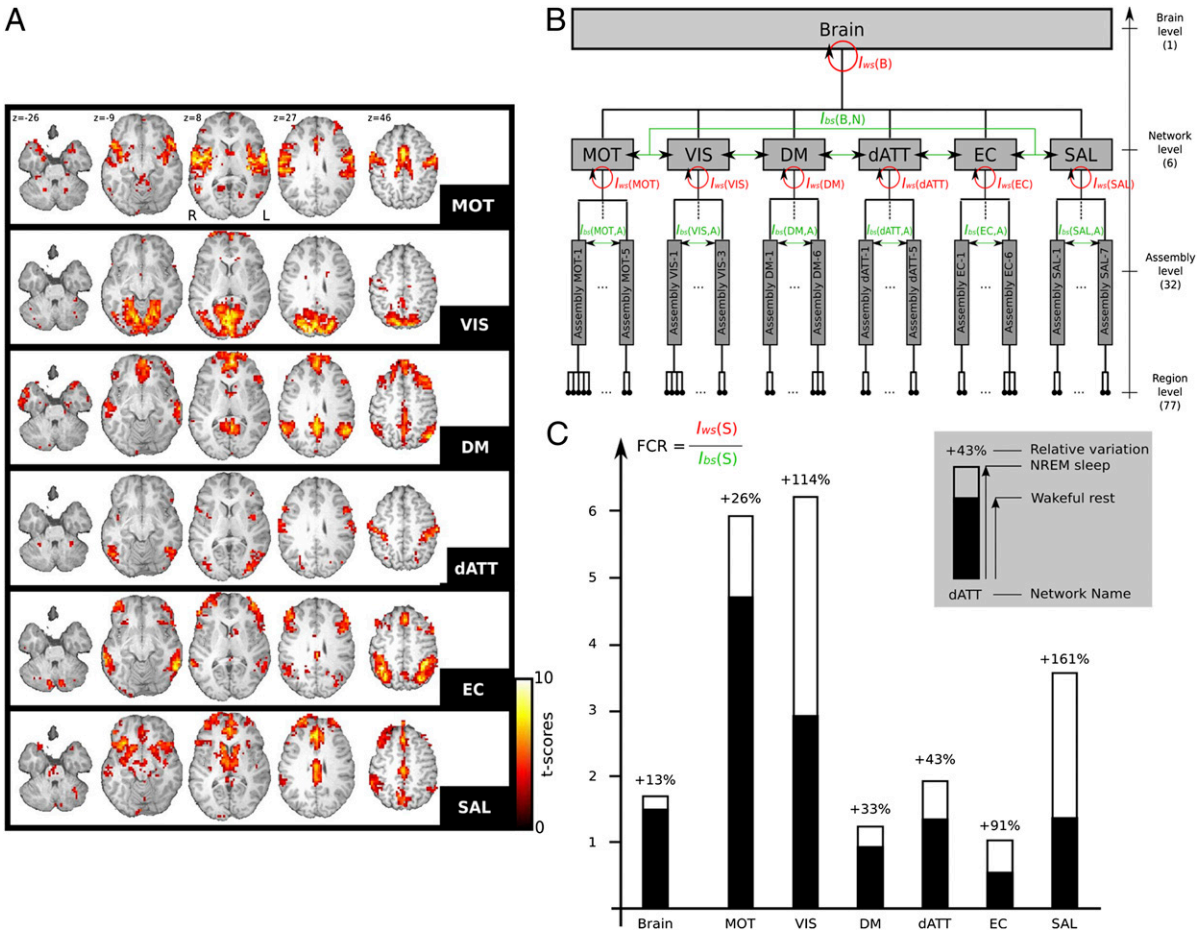


**Fig. 1.** (*A*) The six networks extracted during wakefulness. (*B*) Levels of brain hierarchical integration. (*C*) Increases in functional clustering ratio in the brain and the six networks (all significant with a probability >0.95). Networks: dATT, dorsal attentional; DM, default mode; EC, executive control; MOT, sensorimotor; SAL, salience; VIS, visual.

viduals, both at the brain level and for each network (Table S2). Additional results obtained using graph theory tools also confirmed that brain activity modularity was increased in NREM sleep compared with wakefulness (Fig. 2). These findings indicate that over and above changes in individual network integration or in total brain integration, an essential difference in brain function between wakefulness and NREM sleep consists of increased functional clustering of brain activity into assemblies of homologous areas.

Within each network, we then quantified how much information was exchanged between each node and the rest of the network. We observed a moderate reordering of the importance of the nodes in each network (Fig. 3). Although many areas changed their within-network rank from wakefulness to NREM sleep, the hierarchical organization of the networks was relatively preserved with the transition between states.

**Table 1. Functional clustering ratios (FCR) computed within whole brain and within each network during wakefulness and NREM sleep**

| | Wakefulness | | NREM sleep–wakefulness | Sleep | |
|---|---|---|---|---|---|
| FCR = $I_{ws}/I_{bs}$ | Mean | SD | Variations prob > 0.95 | Mean | SD |
| Brain level vs. networks | | | | | |
| Brain | 1.50 | 0.03 | (+) | 1.70 | 0.03 |
| System level vs. assemblies | | | | | |
| MOT | 4.72 | 0.30 | (+) | 5.95 | 0.37 |
| VIS | 2.92 | 0.27 | (+) | 6.24 | 0.37 |
| DM | 0.93 | 0.06 | (+) | 1.24 | 0.06 |
| dATT | 1.35 | 0.12 | (+) | 1.93 | 0.09 |
| EC | 0.54 | 0.04 | (+) | 1.03 | 0.05 |
| SAL | 1.37 | 0.07 | (+) | 3.57 | 0.18 |

The central column in Tables 1 and 2 indicates the variations with a probability >0.95.

**Table 2. Total brain integration computed within whole brain and within each network during wakefulness and NREM sleep**

| | Wakefulness | | NREM sleep–wakefulness | Sleep | |
|---|---|---|---|---|---|
| $I_{tot}$ | Mean | SD | Variations prob > 0.95 | Mean | SD |
| Brain level vs. networks | | | | | |
| Brain | 5.45 | 0.08 | (+) | 6.37 | 0.07 |
| System level vs. assemblies | | | | | |
| MOT | 0.83 | 0.02 | (–) | 0.76 | 0.02 |
| VIS | 0.32 | 0.02 | (+) | 0.74 | 0.02 |
| DM | 0.56 | 0.02 | (=) | 0.57 | 0.02 |
| dATT | 0.32 | 0.02 | (+) | 0.63 | 0.02 |
| EC | 0.40 | 0.02 | (+) | 0.55 | 0.02 |
| SAL | 0.84 | 0.03 | (–) | 0.73 | 0.02 |

NEUROSCIENCE

**Table 3. Within-subsystems integration values computed for whole brain and for each network during wakefulness and NREM sleep**

| Wakefulness | | | NREM sleep–wakefulness | Sleep | |
|---|---|---|---|---|---|
| $I_{ws}$ | Mean | SD | Variations prob > 0.95 | Mean | SD |
| Brain level vs. networks | | | | | |
| Brain | 3.27 | 0.06 | (+) | 3.98 | 0.05 |
| System level vs. assemblies | | | | | |
| MOT | 0.69 | 0.02 | (=) | 0.66 | 0.02 |
| VIS | 0.24 | 0.01 | (+) | 0.64 | 0.02 |
| DM | 0.27 | 0.01 | (+) | 0.31 | 0.01 |
| dATT | 0.18 | 0.01 | (+) | 0.42 | 0.01 |
| EC | 0.14 | 0.01 | (+) | 0.28 | 0.01 |
| SAL | 0.49 | 0.02 | (+) | 0.57 | 0.02 |

Because the slow oscillation is a fundamental rhythm of NREM sleep potentially associated with a breakdown in cerebral connectivity (11), slow-wave activity (SWA) was regressed to integration measures. Total brain integration was negatively correlated to SWA during NREM sleep (Tables 4 and 5 and Fig. S3). However, there was no significant relation between FCR and SWA (Table 6).

## Discussion

**Content of Consciousness During NREM Sleep.** The current work is based on the theoretical prediction that consciousness is related to the ability of the brain to integrate information. This ability is related to the mathematical construct of complexity, which we approached by computing the functional clustering ratio. To test this hypothesis, we contrasted two polygraphically identified states of vigilance that substantially differ in mental content, namely resting wakefulness and NREM sleep. The reduction of mental content during NREM sleep was confirmed during debriefing after awakening and we are confident that the mental content differed between wakefulness and sleep in our volunteers. Importantly, we do not claim that NREM sleep is associated with a total obliteration of conscious mental representations. The brain remains responsive to external stimuli during NREM sleep (12, 13) and dreams have been reported after NREM sleep awakenings (14). However, the aim of the current paper was not to characterize the neural correlates of these mental representations but rather to contrast brain function during normal wakefulness to that observed during a state of impoverished conscious content such as NREM sleep.

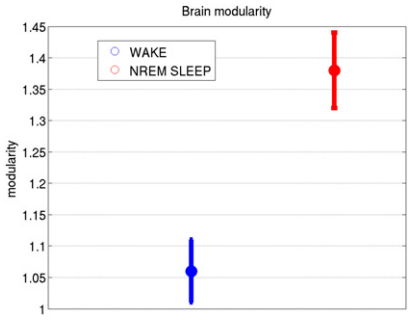


**Fig. 2.** Brain connectivity modularity indexes (group mean result ± SDs) during wakefulness and during NREM sleep. The modularity index, calculated by using the Louvain algorithm, quantifies the degree to which a system may be subdivided into clearly delineated clusters.

**Neurobiological Interpretation of Total-, Within-, and Between-System Integration and Functional Clustering Ratio.** Total integration assesses the sum of information (in the Shannon sense) exchanged between the main functional brain networks and within each of them. Our results show that total integration is larger during NREM sleep than during resting wakefulness. This is an unexpected result. Indeed, although previous studies investigating resting-state fMRI connectivity during states of altered consciousness produced conflicting results (3, 4), they previously mainly revealed a decrease in connectivity. The present results also contrast with previous findings of a globally decreased brain connectivity that has been reported in other altered states of consciousness such as in coma (15) or during anesthesia (ref. 16, in a study performed using the same brain integration quantification technique).

The central point of this paper is to show that beyond these changes in total brain integration, functional interactions are hierarchically modified throughout the brain during NREM sleep, relative to wakefulness. The increase in total brain integration results from a combined increase in both within- and between-network integration. In turn, such changes in integration within each network are due to modifications of the integration both within and between their constituent systems (i.e., their assemblies). In all networks during NREM sleep, the within-system integration becomes proportionally larger than between-system integration, resulting in a consistent increase in FCR. Increased functional clustering of brain activity in small independent modules appears as a general phenomenon and reflects deep, hierarchical modifications in information flow during NREM sleep.

Theoretical considerations predict that increased clustering of brain activity should be associated with a decreased ability to integrate information (6). Information integration should decrease for modular compared with more homogeneously interconnected systems because integrated information is predicted to be maximal for systems that are both highly connected *and* not decomposable in individual subsystems. Integrated information indeed refers to the information generated by the causal interactions in a whole system, over and above the information generated by the parts (17). Increased functional modularity potentially results in a decrease in information integration at the systemic level (2) and, according to the tested hypothesis, this result could then account for the decrease in consciousness during NREM sleep, despite preserved total information processing in the brain. According to this theory, the ability of a system to integrate information appears to be a function not only of the total amount of connectivity in the system, but also of the complexity of the interactions leading to the observed dynamics (5). Functional clustering has been proposed as one empirically tractable measure for the complexity of brain integration, which is supposed to characterize conscious processes (5). Our measure of brain activity functional clustering, defined by the ratio of between- and within-subsystems integration, quantifies the degree of functional segregation of a given system into subsystems. An increase of functional clustering ratio means that the architecture of the system is modified toward a greater proportion of exchanges within subsystems, rather than at the system level—i.e., that the subsystems (networks or assemblies in each network) become more independent from one another. The fact that we observe this phenomenon both at the brain and at the networks level suggests a pervasive presence of this phenomenon during NREM sleep. Additional analyses using classical graph partitioning tools confirmed our result of an increase in brain modularity during NREM sleep compared with wakefulness (Fig. 2). However, to be reliable, such graph theoretical tools have to be applied on a relatively large number of regions. We thus could not apply this same technique to fine network substructure characterization as provided by the use of FCR.

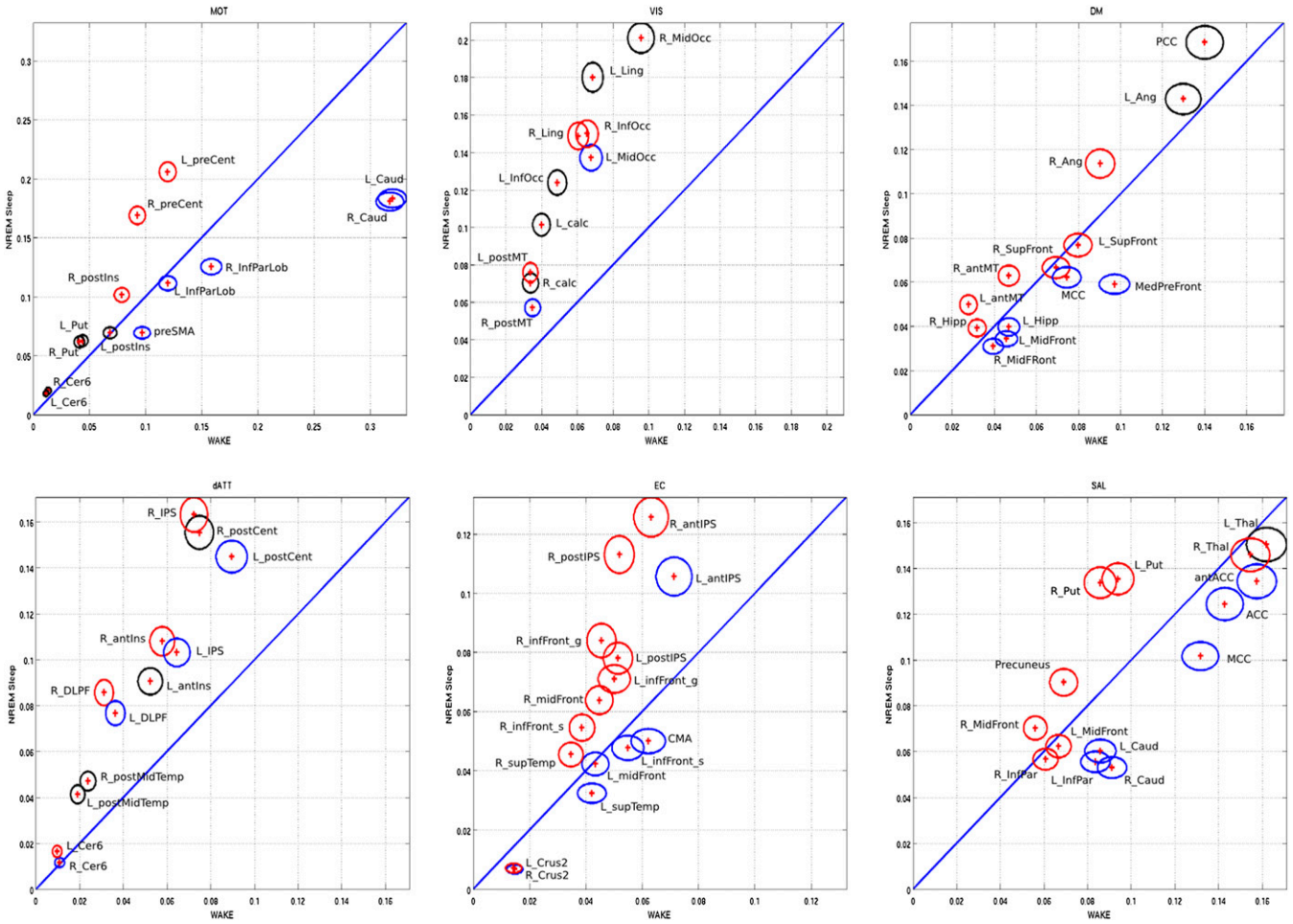


**Fig. 3.** Within-network key node density maps (quantifying the integration between each ROI and the rest of the network) during wakefulness and NREM sleep. The values were sorted for the two conditions to allow one to compare the relative importance of different nodes in each network. Values are displayed on a scatter plot to allow comparison between wakefulness and NREM sleep. The lengths of ellipsoid axes correspond to condition-specific group results SDs. Color codes correspond to the areas for which the rank in the hierarchy is the same (black), higher (blue), or lower (red) during NREM sleep compared with wakefulness. Please refer to Table S1 for ROI coordinates and name abbreviations.

Altogether, these findings are in line with a recent modeling work, showing that reaching high information integration values in a given system requires a subtle balance between functional specialization and integration between the elements constituting the system (6). Following this model, increased clustering of brain activity would result in a decrease in the information integration ability of the system, despite preserved total information processing in the brain. Theoretical predictions indeed state that not only the richness of connectivity, but also its spatial organization matter and that a system that is strongly modular is unlikely to generate high levels of integrated information (6) that has been related to the level of consciousness (2). In this view, investigating general properties of the system, like its modularity, is more relevant to the assessment of the ability of a system to integrate information than merely assessing the amount of information present within this system.

**Changes in the Relative Importance of Key Nodes Within Networks.** In addition to an increased clustering of brain activity, NREM sleep was also associated to a reordering of brain areas in each network—typically placing the network node presenting the highest number of connections during wakefulness at a lowest rank of the hierarchy of areas participating in within-network integration. This result is in line with the proposed role of key integration nodes for normal consciousness (18). However, this modification was not present in all networks (e.g., VIS or DM), and the hierarchical architecture of the networks seemed relatively preserved in NREM sleep compared with wakefulness. Nevertheless, it is possible that these qualitative modifications of within-networks interactions could be

**Table 4. Between-subsystems integration values computed at the whole brain level (between networks) and within each network (between assemblies) during wakefulness and NREM sleep**

| Wakefulness | | | NREM sleep–wakefulness | Sleep | |
|---|---|---|---|---|---|
| $I_{bs}$ | Mean | SD | Variations prob > 0.95 | Mean | SD |
| Brain level vs. networks | | | | | |
| Brain | 2.18 | 0.04 | (+) | 2.39 | 0.03 |
| System level vs. assemblies | | | | | |
| MOT | 0.15 | 0.01 | (–) | 0.11 | 0.01 |
| VIS | 0.08 | 0.01 | (+) | 0.10 | 0.01 |
| DM | 0.29 | 0.01 | (–) | 0.25 | 0.01 |
| dATT | 0.14 | 0.01 | (+) | 0.22 | 0.01 |
| EC | 0.25 | 0.01 | (=) | 0.27 | 0.01 |
| SAL | 0.36 | 0.02 | (–) | 0.16 | 0.01 |

**Table 5. Correlation coefficient *R* between total Integration (*I*) and slow-wave activity during NREM sleep for brain and the six networks**

| $I_{tot}$ vs. SWA | *R* | *P* value (two-tailed) |
|---|---|---|
| Brain level vs. networks | | |
| Brain | −0.42 | 0.0037* |
| Network level vs. assemblies | | |
| MOT | −0.25 | 0.0938 |
| VIS | −0.07 | 0.6439 |
| DM | −0.32 | 0.0301* |
| dATT | −0.43 | 0.0029* |
| EC | −0.36 | 0.0140* |
| SAL | −0.43 | 0.0029* |

*Significant correlation with a *P* value <0.05.

another contributing mechanism to altered consciousness during NREM sleep.

**Brain Integration, Slow Oscillation, and Influence of Other Unidentified Factors.** Changes in brain integration during NREM sleep seem to result from two antagonistic influences. On the one hand, integration decreases in proportion to SWA. This result is consistent with a breakdown of brain connectivity resulting from the bistable neural response associated with the slow oscillation, the fundamental NREM sleep rhythm (11). However, this slow oscillation, as assessed by SWA, does not account for the global increase in total brain integration or for the pervasive increase in functional clustering. With deepening of sleep, a decrease of total brain connectivity could be an additive mechanism to functional clustering, leading to a decrease in the brain's ability to generate conscious perception. Indeed, theoretically, if not only the system becomes more modular, but also the total connectivity of the system further diminishes, information integration is likely to decrease even more at the system level (6).

The processes underlying the increase in total brain integration and functional clustering remain unidentified. NREM sleep is associated with considerable changes in aminergic and peptidergic neuromodulation (19). Although a change in neuromodulation is a plausible hypothesis, its impact on regional cortical function remains unknown. An alternative hypothesis would assume that total brain integration and functional clustering result from changes in infra-slow oscillations. This hypothesis is supported by a number of experimental data. Infra-slow oscillations (<0.1 Hz) are known to modulate cortical activity in animals (20, 21) as well as human behavior (22) and human brain activity during both wakefulness (23) and sleep (24). Moreover, infra-slow oscillations of neural activity are also consistent with spontaneous fluctuations of fMRI blood oxygen level dependent signal during resting state in animals (21) and similar oscillations are observed in human fMRI recordings (25). Critically, the infra-slow oscillations, as measured in humans by magneto-encephalography, are noticeably stronger during sleep than during resting wakefulness and tend to synchronize over a long spatial distance, especially between bilaterally homologous regions in opposite hemispheres (26). These functional features are remarkably consistent with our fMRI findings: an enhanced integration between homologous brain areas during NREM sleep, relative to wakefulness. From a functional standpoint, infra-slow oscillations are thought to coordinate thalamo-cortical processing in distant brain regions (21), thereby promoting functional integration. The mechanisms of infra-slow oscillations are not yet identified but seem to be related to modulation of cortical activity by brainstem nuclei (27), as well as to network properties of thalamic neurons possibly driven by nonneural mechanisms (28).

In conclusion, we speculate that part of our results can be explained by the modulation of brain function by infra-slow oscillations during NREM sleep. The hierarchical modifications in the organization of brain integration, reflected as an increased functional clustering, support the hypothesis that the altered conscious content during NREM sleep is related to a decrease in the ability of the brain to integrate information.

**Table 6. Correlation coefficient *R* between functional clustering ratios (FCR) for brain and the six networks**

| FCR vs. SWA | *R* | *P* value (two-tailed) |
|---|---|---|
| Brain level vs. networks | | |
| Brain | −0.11 | 0.4668 |
| Network level vs. assemblies | | |
| MOT | 0.00 | 0.9879 |
| VIS | 0.15 | 0.3197 |
| DM | −0.02 | 0.8950 |
| dATT | −0.15 | 0.3197 |
| EC | −0.06 | 0.6920 |
| SAL | 0.00 | 0.9968 |

## Materials and Methods

**Population and Experimental Design.** Young healthy participants ($n$ = 25; 11 females; age range, 18–25 y; mean age, 21.96 y) were recruited by advertisement. From this group, 13 participants maintained periods of steady NREM sleep, and thus the data of these subjects were used in this study. None were on medication or sleep deprived (*SI Materials and Methods* and *SI Results*). After the experimental session, volunteers were asked to report the occurrence of relevant thoughts, mentation, or dreams that they might have had during scanning.

**EEG Acquisition and Analysis.** EEG was recorded using two MR-compatible 32-channel amplifiers and an MR-compatible EEG cap with 64 ring-type electrodes (*SI Materials and Methods*). Sleep staging of scanning artifacts-corrected EEG (*SI Materials and Methods*) followed standard criteria and identified periods of stages 2–4 NREM sleep, free of any artifact, during which the EEG and fMRI data were analyzed. EEGs were subjected to spectral analysis on a frontal electrode (Fz), using a Fast Fourier Transform (4-s window, 2-s steps, Hanning window), resulting in a 0.25-Hz spectral resolution. SWA activity corresponded to the power within the 0.5- to 4-Hz band. Relative power was obtained by normalizing absolute power to total power. Sleep parameters are summarized in Table S3.

**fMRI Data Acquisition and Analysis.** Functional MRI time series were acquired using a 3-Tesla MR scanner (Allegra; Siemens). Multislice $T_2$*-weighted fMRI images and a structural $T_1$-weighted 3D Magnetization Prepared RApid Gradient Echo (MP-RAGE) sequence were acquired from all subjects. From this dataset, we extracted consecutive volumes recorded during wakefulness and NREM sleep. To do so, we chose the longest series during the two conditions for each subject (limited to a maximum of 300 vol for computational reasons). One hundred fifty-six to 300 vol were selected for wakefulness series (total of 33 runs) and 132–300 vol for NREM sleep series (total of 46 runs).

***Network and assembly identification. Overview.*** Using all datasets acquired during wakefulness for all subjects, functional networks whose spatial structure was reproducible across subjects were identified using the NEDICA method (29) freely available in NetBrainWork (http://www.imed.jussieu.fr/fr/equipes/e1/netbrainwork/netbrainwork.php) (*SI Materials and Methods*). The latter comprised six functional networks representing an incomplete partition of the whole brain (VIS, MOT, DM, dATT, EC, and SAL networks; cf. refs. 8–10). We defined the ROIs from the peaks of the *t*-maps of the functional networks.

Before extracting BOLD signal within ROIs, structured noise (related to, e.g., respiration, heartbeat, and movements) was reduced with CORSICA (30) (*SI Materials and Methods*). Complementary analyses were performed to rule out that differences in within-session movement amplitude could explain our results (*SI Results*, Fig. S4, and Tables S4–S7).

***Networks parcellation into assemblies.*** After preprocessing and removal of structured noise, all functional datasets were registered into the MNI standardized space. The spatial average BOLD signals within each ROI were then extracted for all subjects and for the two conditions (wakefulness and

NREM sleep). The averaged correlation matrix was computed for each network during NREM sleep and thresholded at $P < 0.05$. The thresholded correlation structure was computed for each network during NREM sleep and their structure was assessed by a hierarchical clustering that maximized intraclass similarity, defined as sqrt(1 − $r$), where $r$ was the correlation between two regions. By thresholding the similarity trees, the networks were divided into assemblies of areas. The results presented in the main text are based on a qualitative neuroanatomy-based threshold (Fig. S2, *SI Materials and Methods*). Similar results were obtained using another data-driven partition of the networks, thresholding the similarity trees at the level of the highest increase of intracluster distance (Fig. S5 and Table S8). Results were not modified by using several alternative approaches a sub-systems organization defined from NREM sleep data (Table S10) or by using wakefulness sub-systems organization in the hierarchical clustering (Table S11).

***Functional clustering ratio.*** To quantify functional interactions within and between networks during the two conditions we used total correlation (31), a measure also known as integration in neurocomputing (32) and fMRI data analysis (33) (*SI Materials and Methods*).

We defined the FCR as the ratio between the integration within subsystems ($I_{ws}$), compared with the integration present between these subsystems ($I_{bs}$). It is a measure of clustering inside a given system because an increase in FCR indicates that subsystems become functionally more independent of each other. In other words, it quantifies the degree of functional segregation of a given system into subsystems:

$$\mathrm{FCR} = I_{ws}/I_{bs}. \quad [1]$$

***Bayesian estimation and comparison between conditions.*** Probable values of integration and FCR were inferred from the data using a fixed-effects group approach (33) and a Bayesian group analysis with numerical sampling scheme (1,000 samples per estimate) (34) for these analyses (*SI Materials and Methods*). During the sampling procedure to estimate the group covariance matrix for each group (wakefulness and NREM sleep), a covariance matrix is estimated for each individual. Thus, similarly to the group analysis, we compared the resulting 1,000 estimates of FCR at the individual level between wakefulness and NREM sleep, at the brain level, and for each network. As for group analyses, a probability of difference >0.95 was considered significant.

***Brain modularity computation during wakefulness and NREM sleep.*** From the group correlation matrices computed during wakefulness and NREM sleep, we defined a weighted graph where the weights between nodes $i$ and $j$ were $(1 - rij)/(1 + rij)$. The modularity index, which quantifies the degree to which a system may be subdivided in clearly delineated clusters, was calculated using the Louvain algorithm (35) provided in the Brain Connectivity Toolbox (http://www.brain-connectivity-toolbox.net) (36).

***Node density maps in wakefulness and NREM sleep datasets.*** Within each network, we computed the integration between each ROI and the rest of the network (i.e., the other ROIs of the same network) during wakefulness and NREM sleep. These values were sorted for the two conditions to allow one to compare the relative importance of each node in the network. Fig. 3 displays integration values and SD for each node of each network, hierarchically ordered in wakefulness and NREM sleep. Ellipsoids correspond to SDs of integration value, conjointly displayed for each area for wakefulness and NREM sleep datasets.

***SWA and functional integration.*** SWA was evaluated for each NREM run as the EEG spectral power within the (0.5–4 Hz) frequency band relative to the total spectral power. This measure was regressed to the interaction measures of interest ($I$, $I_{ws}$, $I_{bs}$, and FCR) computed in the corresponding fMRI sessions. Correlation was considered significant at $P < 0.05$.

**ACKNOWLEDGMENTS.** This research was supported by the Belgian Fonds National de la Recherche Scientifique, Fondation Médicale Reine Elisabeth, and Research Fund of the University of Liège. M.B., S.L., and P.M. are supported by the Fonds National de la Recherche Scientifique. J.D. is also supported by European Sleep Research Grant 2008 of the European Sleep Research Society. M.S. was supported by an Erwin Schrödinger fellowship of the Austrian Science Fund (J2470-B02).

1. Hobson JA, Pace-Schott EF, Stickgold R (2000) Dreaming and the brain: Toward a cognitive neuroscience of conscious states. *Behav Brain Sci* 23:793–842, discussion 904–1121.
2. Tononi G (2005) Consciousness, information integration, and the brain. *Prog Brain Res* 150:109–126.
3. Larson-Prior LJ, et al. (2009) Cortical network functional connectivity in the descent to sleep. *Proc Natl Acad Sci USA* 106:4489–4494.
4. Spoormaker VI, et al. (2010) Development of a large-scale functional brain network during human non-rapid eye movement sleep. *J Neurosci* 30:11379–11387.
5. Tononi G, Edelman GM (1998) Consciousness and complexity. *Science* 282:1846–1851.
6. Balduzzi D, Tononi G (2008) Integrated information in discrete dynamical systems: Motivation and theoretical framework. *PLoS Comput Biol*, 10.1371/journal.pcbi.1000091.
7. Nir Y, et al. (2007) Coupling between neuronal firing rate, gamma LFP, and BOLD fMRI is related to interneuronal correlations. *Curr Biol* 17:1275–1285.
8. Beckmann CF, DeLuca M, Devlin JT, Smith SM (2005) Investigations into resting-state connectivity using independent component analysis. *Philos Trans R Soc Lond B Biol Sci* 360:1001–1013.
9. Damoiseaux JS, et al. (2006) Consistent resting-state networks across healthy subjects. *Proc Natl Acad Sci USA* 103:13848–13853.
10. Seeley WW, et al. (2007) Dissociable intrinsic connectivity networks for salience processing and executive control. *J Neurosci* 27:2349–2356.
11. Massimini M, et al. (2005) Breakdown of cortical effective connectivity during sleep. *Science* 309:2228–2232.
12. Dang-Vu TT, et al. (2011) Interplay between spontaneous and induced brain activity during human non-rapid eye movement sleep. *Proc Natl Acad Sci USA* 108: 15438–15443.
13. Bastuji H, García-Larrea L (1999) Evoked potentials as a tool for the investigation of human sleep. *Sleep Med Rev* 3:23–45.
14. Antrobus J (1983) REM and NREM sleep reports: Comparison of word frequencies by cognitive classes. *Psychophysiology* 20:562–568.
15. Vanhaudenhuyse A, et al. (2010) Default network connectivity reflects the level of consciousness in non-communicative brain-damaged patients. *Brain* 133:161–171.
16. Schrouff J, et al. (2011) Brain functional integration decreases during propofol-induced loss of consciousness. *Neuroimage* 57(1):198–205.
17. Tononi G (2008) Consciousness as integrated information: A provisional manifesto. *Biol Bull* 215:216–242.
18. Boly M (2011) Measuring the fading consciousness in the human brain. *Curr Opin Neurol* 24:394–400.
19. Steriade M, McCarley RW (2005) *Brain Control of Wakefulness and Sleep* (Kluwer Academic, New York).
20. Aladjalova NA (1957) Infra-slow rhythmic oscillations of the steady potential of the cerebral cortex. *Nature* 179:957–959.
21. Leopold DA, Murayama Y, Logothetis NK (2003) Very slow activity fluctuations in monkey visual cortex: Implications for functional brain imaging. *Cereb Cortex* 13: 422–433.
22. Monto S, Palva S, Voipio J, Palva JM (2008) Very slow EEG fluctuations predict the dynamics of stimulus detection and oscillation amplitudes in humans. *J Neurosci* 28: 8268–8272.
23. Palva S, Linkenkaer-Hansen K, Näätänen R, Palva JM (2005) Early neural correlates of conscious somatosensory perception. *J Neurosci* 25:5248–5258.
24. Vanhatalo S, et al. (2004) Infraslow oscillations modulate excitability and interictal epileptic activity in the human cortex during sleep. *Proc Natl Acad Sci USA* 101: 5053–5057.
25. Fox MD, Raichle ME (2007) Spontaneous fluctuations in brain activity observed with functional magnetic resonance imaging. *Nat Rev Neurosci* 8:700–711.
26. Liu Z, Fukunaga M, de Zwart JA, Duyn JH (2010) Large-scale spontaneous fluctuations and correlations in brain electrical activity observed with magnetoencephalography. *Neuroimage* 51:102–111.
27. Usher M, Cohen JD, Servan-Schreiber D, Rajkowski J, Aston-Jones G (1999) The role of locus coeruleus in the regulation of cognitive performance. *Science* 283:549–554.
28. Lörincz ML, Geall F, Bao Y, Crunelli V, Hughes SW (2009) ATP-dependent infra-slow (<0.1 Hz) oscillations in thalamic networks. *PLoS ONE*, 10.1371/journal.pone.0004447.
29. Perlbarg V, et al. (2008) NEDICA: Detection of group functional networks in fMRI using spatial independent component analysis. *Proceedings of the 5th IEEE International Symposium on Biomedical Imaging: From Nano to Macro, 2008* (Institute of Electrical and Electronics Engineers, Paris), pp 1247–1250.
30. Perlbarg V, et al. (2007) CORSICA: Correction of structured noise in fMRI by automatic identification of ICA components. *Magn Reson Imaging* 25:35–46.
31. Watanabe S (1960) Information theoretical analysis of multivariate correlation. *IBM J Res Dev* 4((1)):66–82.
32. Tononi G, Sporns O, Edelman GM (1994) A measure for brain complexity: Relating functional segregation and integration in the nervous system. *Proc Natl Acad Sci USA* 91:5033–5037.
33. Marrelec G, et al. (2008) Regions, systems, and the brain: Hierarchical measures of functional integration in fMRI. *Med Image Anal* 12:484–496.
34. Marrelec G, et al. (2006) Partial correlation for functional brain interactivity investigation in functional MRI. *Neuroimage* 32:228–237.
35. Blondel VD, Guillaume JL, Lambiotte R, Lefebvre E (2008) Fast unfolding of communities in large networks. *J Stat Mech*, 10.1088/1742-5468/2008/10/P10008.
36. Rubinov M, Sporns O (2010) Complex network measures of brain connectivity: Uses and interpretations. *Neuroimage* 52:1059–1069.

# Supporting Information

## Boly et al. 10.1073/pnas.1111133109

### SI Materials and Methods

**Population and Experimental Design.** Healthy, young participants ($n$ = 25; 11 females; age range, 18–25 y; mean age, 21.96 y) were recruited by advertisement. From this group, 13 participants could maintain periods of steady NREM sleep—the data of these subjects are used in this study. A semistructured interview established the absence of medical, traumatic, or psychiatric history or of sleep disorders. All participants were nonsmokers and moderate caffeine and alcohol consumers. None were on medication. None had worked on night shifts during the last year or traveled through more than one time zone during the last 2 mo. Extreme morning and evening types, as assessed by the Horne–Ostberg Questionnaire (1), were not included. None complained of excessive daytime sleepiness as assessed by the Epworth Sleepiness Scale (2) and of sleep disturbances as determined by the Pittsburgh Sleep Quality Index Questionnaire (3). All participants had normal scores in the 21-item Beck Anxiety Inventory and the 21-item Beck Depression Inventory II (4). Participants gave their written informed consent and received a financial compensation for their participation. The study was approved by the Ethics Committee of the Faculty of Medicine of the University of Liège. Volunteers followed a 4-d constant sleep schedule before their first visit to the laboratory and were not sleep deprived. Compliance to the schedule was assessed using wrist actigraphy (Actiwatch; Cambridge Neuroscience) and sleep diaries. Volunteers were requested to refrain from all caffeine and alcohol-containing beverages and intense physical activity for 3 d before participating in the study. On the experimental evening, volunteers reported to the laboratory at 9:00 PM. Actigraphy and sleep diaries were checked for compliance with the sleep schedule. These non-sleep–deprived volunteers were scanned during the first half of the night, starting at around midnight. They stayed until they indicated by a button press that they would like to go out or for a maximum of 4,000 scans (~164 min). The number of scans acquired varied between 534 and 4,000 [2,565 ± 950 scans or 105.2 min ± 39.00 min (mean ± SD)]. After the experimental session, volunteers were asked to report the occurrence of relevant thoughts, mentation, or dreams that they might have had during scanning.

**EEG Acquisition.** EEG was recorded using two MR-compatible 32-channel amplifiers (Brainamp MR plus; Brain Products) and an MR-compatible EEG cap (Braincap MR; Falk Minow Services) with 64 ring-type electrodes. The EEG cap included 62 scalp electrodes that were online referenced to a frontocentral electrode (FCz), as well as one electrooculogram (EOG) and one electrocardiogram (ECG) channel. Using abrasive electrode paste (ABRALYT 2000; FMS), electrode–skin impedance was kept below 5 kOhm in addition to the 5-kOhm resistor built into the electrodes. To avoid movement-related EEG artifacts, subjects' heads were immobilized in the head coil by a vacuum pad. EEG was digitized at a 5,000-Hz sampling rate with a 500-nV resolution. Data were analog filtered by a band-limiter low-pass filter at 250 Hz (30 dB per octave) and a high-pass filter with 10-s time constant corresponding to a high-pass frequency of 0.0159 Hz. Data were transferred outside the scanner room through fiber-optic cables to a personal computer where the EEG system running Vision Recorder Software v1.03 (Brain Products) was synchronized to the scanner clock. Sleep EEG was monitored online with BrainProducts RecView Software. For analysis, EEG data were low-pass filtered (finite impulse response filter, −36 dB at 70 Hz), down-sampled to 250 Hz, and rereferenced to linked mastoids. Scanner artifacts were removed in Vision Analyzer, using an adaptive average subtraction. Ballistocardiographic artifacts were removed using an algorithm based on independent component analysis (ICA).

**fMRI Data Acquisition.** Functional MRI time series were acquired using a 3-Tesla MR scanner (Allegra; Siemens). Multislice $T_2$*-weighted fMRI images were obtained with a gradient echo-planar sequence using axial slice orientation [32 slices; voxel size, 3 × 3.4 × 3 mm$^3$; matrix size, 64 × 64 × 32; repetition time (TR) = 2,460 ms; echo time (TE) = 40 ms; flip angle = 90°; field of view (FOV) = 220 mm; delay = 0]. The three initial scans were discarded to avoid magnetic saturation effects. A structural $T_1$-weighted 3D Magnetization Prepared RApid Gradient Echo (MP-RAGE) sequence (TR = 1,960 ms; TE = 4.43 ms; inversion time, 1,100 ms; FOV = 230 × 173 mm$^2$; matrix size, 256 × 192 × 176; voxel size, 0.9 × 0.9 × 0.9 mm$^3$) was also acquired in all subjects. Part of this dataset has been used to characterize the neural correlates of NREM sleep spindles (5) and slow waves (6) and has already been reported but the present study, resorting to completely different analytic methods, does not overlap with these earlier reports.

**Network identification.** Forty spatially independent components were first calculated for each subject fMRI wakefulness data set, using the Infomax ICA algorithm (7). After registration into the Montreal Neurological Institute standardized space, the 40 components × 13 subjects were then clustered using a hierarchical clustering algorithm. Networks were defined from the similarity tree as they were the most representative of the population. A group $t$ map was associated with each network class. The maps involving regions distributed around blood vessels, sinus, ventricles, or the outline of the brain were discarded and the other ones, whose spatial structures were located in gray matter, were used for subsequent analysis.

We defined the ROIs from the peaks of the t-maps of the functional networks. A semiautomatic procedure was used. An automated selection algorithm identified the maximal peaks of $t$ values for each network at the population level. The peaks were then manually verified for each network, leaving the automatic selection mostly unchanged. The ROIs were then built from these selected peaks, using a region-growing algorithm that recursively added to the region the adjacent voxel with the highest $t$ score. The algorithm stopped when the region was of 10-voxel size.

**Removal of structured noise.** Before extracting BOLD signal within ROIs, structured noise (related to, e.g., respiration, heartbeat, and movements) was reduced with CORSICA (7), which uses the ability of spatial ICA decomposition to separate processes related to structured noise from the others. Automatic selection of noise-related components was based on their spatial distribution. CORSICA identifies maps with a spatial distribution of $Z$ values maximal around ventricles or edges of the brain as likely movements or physiological noise and subtracts these components of signal from the original data.

**Networks parcellation into assemblies.** The results presented in the main text are based on a qualitative neuroanatomy-based threshold (Fig. S2). Recent structural connectivity measures in humans reported that between 9% and 14% of all binary connections are interhemispheric (7). A consistent aspect of resting -state fMRI connectivity is also the correlation across homotopic sides of the two hemispheres (8–11). In line with these considerations, we

selected the clustering threshold to partition each network into assemblies including homotopic areas from both hemispheres. Similar results were obtained using another data-driven partition of the networks, thresholding the similarity tress at the level of highest increase of intracluster distance (Fig. S5, Table S9).

**Computation of integration.** Considering $N$ ROIs characterized by their mean time courses $y = (y_1, \ldots, y_N)$ gathered into $K$ systems $S = \{S_1, \ldots, S_K\}$, integration is defined as

$$I[y_1, \ldots, y_N] = \sum_{n=1}^{N} H(p(y_n)) - H(p(y_1, \ldots, y_N)), \qquad [1]$$

where $H(.)$ is the entropy measure.

For multivariate normal data with mean *mu* and covariance matrix Sigma, entropy can easily be computed as

$$H(p(y)) = 1/2 \ln(|\text{Sigma}|), \qquad [2]$$

where $|.|$ stands for the determinant.

Interestingly, the total integration can be decomposed, according the organization of ROIs into systems, as the sum of between-system integration and within-system integration:

$$I[y_1, \ldots, y_N] = I_{\text{bs}} + I_{\text{ws}}, \text{ with } I_{\text{bs}} = I\left[y_{S_1}, \ldots, y_{S_K}\right] \text{ and } I_{\text{ws}} = \sum_{k=1}^{K} I\left((y_n)_{n \in S_k}\right).$$

**Bayesian estimation and comparison between conditions.** Probable values of integration and FCR were inferred from data as follows. Using a Bayesian group analysis with numerical sampling scheme, we first obtained $L = 1{,}000$ samples $(\text{Sigma}^l)_{l=1,\ldots,L}$ from the posterior distribution of the group covariance matrix in either condition (wakefulness or NREM sleep). From each sample $\text{Sigma}^l$, we computed the corresponding values of integration ($I_{\text{ws}}$ and $I_{\text{bs}}$) and FCR using Eqs. **1**–**3**. For each measure and condition, we therefore obtained a frequency histogram that, by construction, approximated the posterior distribution of that measure given the data. The samples were then used to provide approximations of either statistics (e.g., mean and SD approximated as their sample counterparts) or probabilities [e.g., probability of an increase between wakefulness (W) and NREM sleep] approximated as the frequency of that increase observed in the sample. The values of integration and FCR were inferred in a Bayesian framework. For example, it was possible to approximate the posterior probability $p(A|y)$ of the assertion $A = \{\text{FCR\_network1\_wake} > \text{FCR\_network1\_NREMsleep}\}$ given the mean time courses within ROIs $y$. $p(A|y)$ is approximated using a Bayesian group analysis with numerical sampling scheme as detailed in ref. 39: $L = 1{,}000$ samples, $(\text{Sigma}^l)_{l=1,\ldots,L}$ from the posterior distribution of the group covariance matrix in either condition (wakefulness or NREM sleep) were obtained from the data. Finally, $p(A|y)$ was approximated by

$$\{\text{FCR\_network1\_wake}\{l\} > FCR\_\text{network1\_sleep}\{l\}\}/L,$$

where $l = (1, \ldots, L)$ and # stands for the cardinal function of a set. This procedure was already used in refs. 14 and 15.

## SI Results

**Influence of Region-of-Interest (ROI) Selection and Hierarchical Clustering Procedure on Functional Clustering Ratio (FCR) Changes Between Wakefulness and NREM Sleep.** We performed complementary analyses to ensure that our results were not biased by the analytic procedures [independent component analysis (ICA) system identification based on wakefulness data; hierarchical clustering in subsystems based on NREM sleep data]. First, we computed ICA from NREM sleep data. Eight networks consistently observed across subjects were identified and compared with those identified from wakefulness data (Fig. S1). This comparison showed the following:

Three networks were spatially similar (spatial correlation up to 0.7) between wakefulness and NREM sleep: default mode (DM), attentional (ATT), and executive control (EC). Our results on FCR were therefore not modified for these systems.

Two networks were split into two parts from wakefulness to NREM sleep: motor (MOT) into MOT1 and MOT2 and visual (VIS) into VIS1 and VIS2. By directly using these results to define the system–subsystems organizations for MOT and VIS, we showed that the FCR still increased from wakefulness to NREM sleep (Table S9).

One network could not be considered spatially identical between wakefulness and NREM sleep: salience (SAL). We then defined specific system–subsystems organization for the SAL system identified from NREM sleep data. We showed once again that FCR increased from wakefulness to NREM sleep (Table S9).

Second, we examined whether the hierarchical clustering originally conducted on NREM sleep data could have influenced the observed change in FCR between states of vigilance. We defined subsystems by computing hierarchical clustering on wakefulness data, instead of NREM sleep data. The functional clustering ratio still increased from wakefulness to NREM sleep using this new set of subsystems (Table S10).

**Influence of Movement on FCR Computation During NREM Sleep and Wakefulness.** As described in ref. 13, we computed for each subject and each session the mean motion metric from the estimated translation and rotation parameters from the rigid body correction (Statistical Parametric Mapping version 5). To do so, we computed for each brain volume the root-mean square (RMS) of the translation parameters and of the rotation parameters (expressed in millimeters). Then, the mean motion of a time series is calculated as the mean of the absolute RMS difference between adjacent volumes (for translation and rotation independently). Rotation and translation movement amplitude was not statistically different in sleep compared with wakefulness (Fig. S4). In an additional analysis, we added to the main FCR and integration computation a preprocessing step to remove residual variance induced by movement to the areas' time series. This step consists of regressing out the six parameters obtained by rigid body and head motion correction from each region-of-interest time course after their computation. The finding of diffuse increase in FCR, both at the brain level and at each network level, present during sleep compared with wakefulness, remained unchanged after this procedure (Tables S4–S7).


1. Horne JA, Ostberg O (1976) A self-assessment questionnaire to determine morningness-eveningness in human circadian rhythms. *Int J Chronobiol* 4:97–110.
2. Johns MW (1991) A new method for measuring daytime sleepiness: The Epworth sleepiness scale. *Sleep* 14:540–545.
3. Buysse DJ, Reynolds CF, 3rd, Monk TH, Berman SR, Kupfer DJ (1989) The Pittsburgh Sleep Quality Index: A new instrument for psychiatric practice and research. *Psychiatry Res* 28:193–213.
4. Beck AT, Epstein N, Brown G, Steer RA (1988) An inventory for measuring clinical anxiety: Psychometric properties. *J Consult Clin Psychol* 56:893–897.
5. Schabus M, et al. (2007) Hemodynamic cerebral correlates of sleep spindles during human non-rapid eye movement sleep. *Proc Natl Acad Sci USA* 104:13164–13169.
6. Dang-Vu TT, et al. (2008) Spontaneous neural activity during human slow wave sleep. *Proc Natl Acad Sci USA* 105:15160–15165.
7. McKeown MJ, et al. (1998) Analysis of fMRI data by blind separation into independent spatial components. *Hum Brain Mapp* 6:160–188.

8. Perlbarg V, et al. (2007) CORSICA: Correction of structured noise in fMRI by automatic identification of ICA components. *Magn Reson Imaging* 25:35–46.
9. Hagmann P, et al. (2008) Mapping the structural core of human cerebral cortex. *PLoS Biol*, 10.1371/journal.pbio.0060159.
10. Nir Y, Hasson U, Levy I, Yeshurun Y, Malach R (2006) Widespread functional connectivity and fMRI fluctuations in human visual cortex in the absence of visual stimulation. *Neuroimage* 30:1313–1324.
11. Fox MD, Snyder AZ, Zacks JM, Raichle ME (2006) Coherent spontaneous activity accounts for trial-to-trial variability in human evoked brain responses. *Nat Neurosci* 9:23–25.
12. Biswal B, Yetkin FZ, Haughton VM, Hyde JS (1995) Functional connectivity in the motor cortex of resting human brain using echo-planar MRI. *Magn Reson Med* 34: 537–541.
13. Van Dijk KR, Sabuncu MR, Buckner RL (2012) The influence of head motion on intrinsic functional connectivity MRI. *Neuroimage* 59:431–438.
14. Schrouff J, et al. (2011) Brain functional integration decreases during propofol-induced loss of consciousness. *Neuroimage* 57(1):198–205.
15. Coynel D, et al. (2010) Dynamics of motor-related functional integration during motor sequence learning. *Neuroimage* 49:759–766.

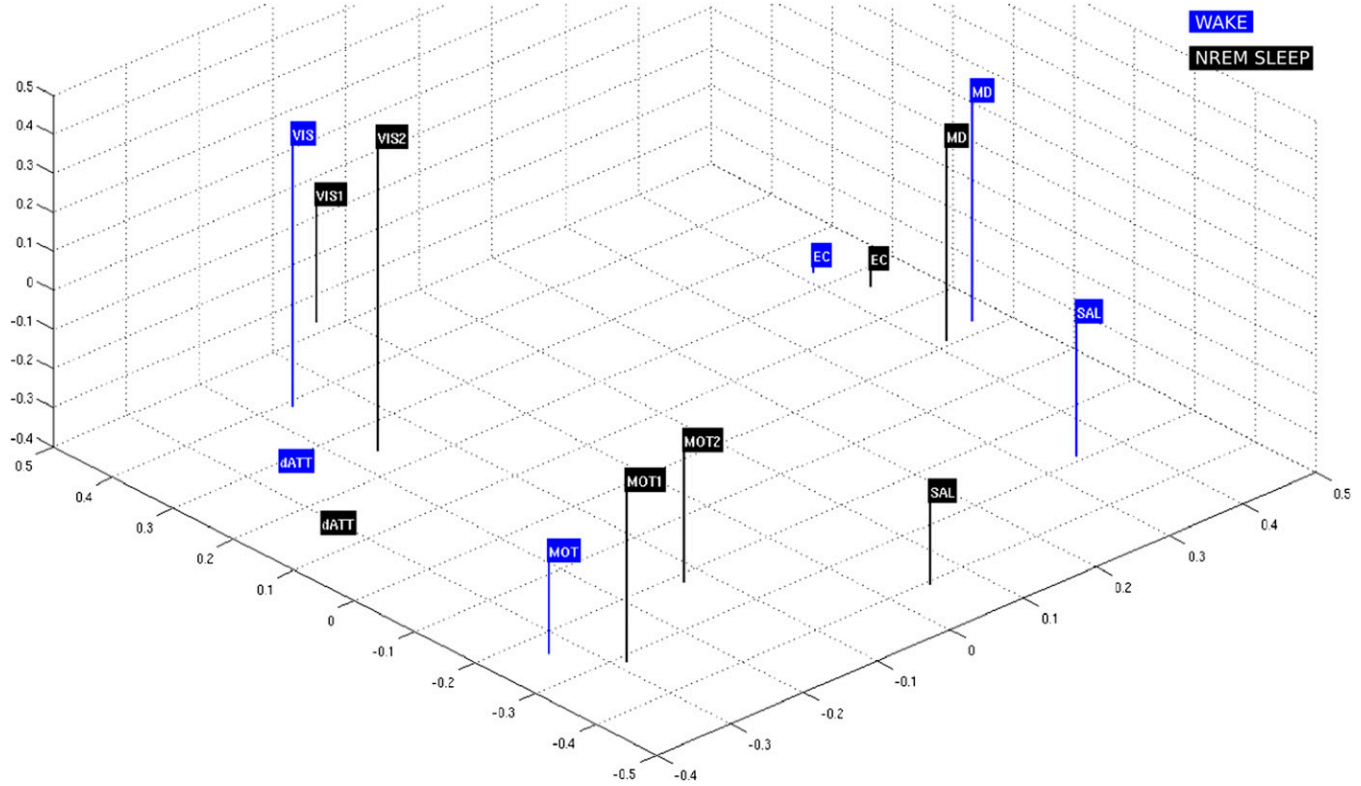


**Fig. S1.** Multidimensional scaling representation of relative spatial similarities of ICA networks. Blue flags: the six wakefulness networks derived from waking data. Black flags: the eight networks derived from NREM sleep data.

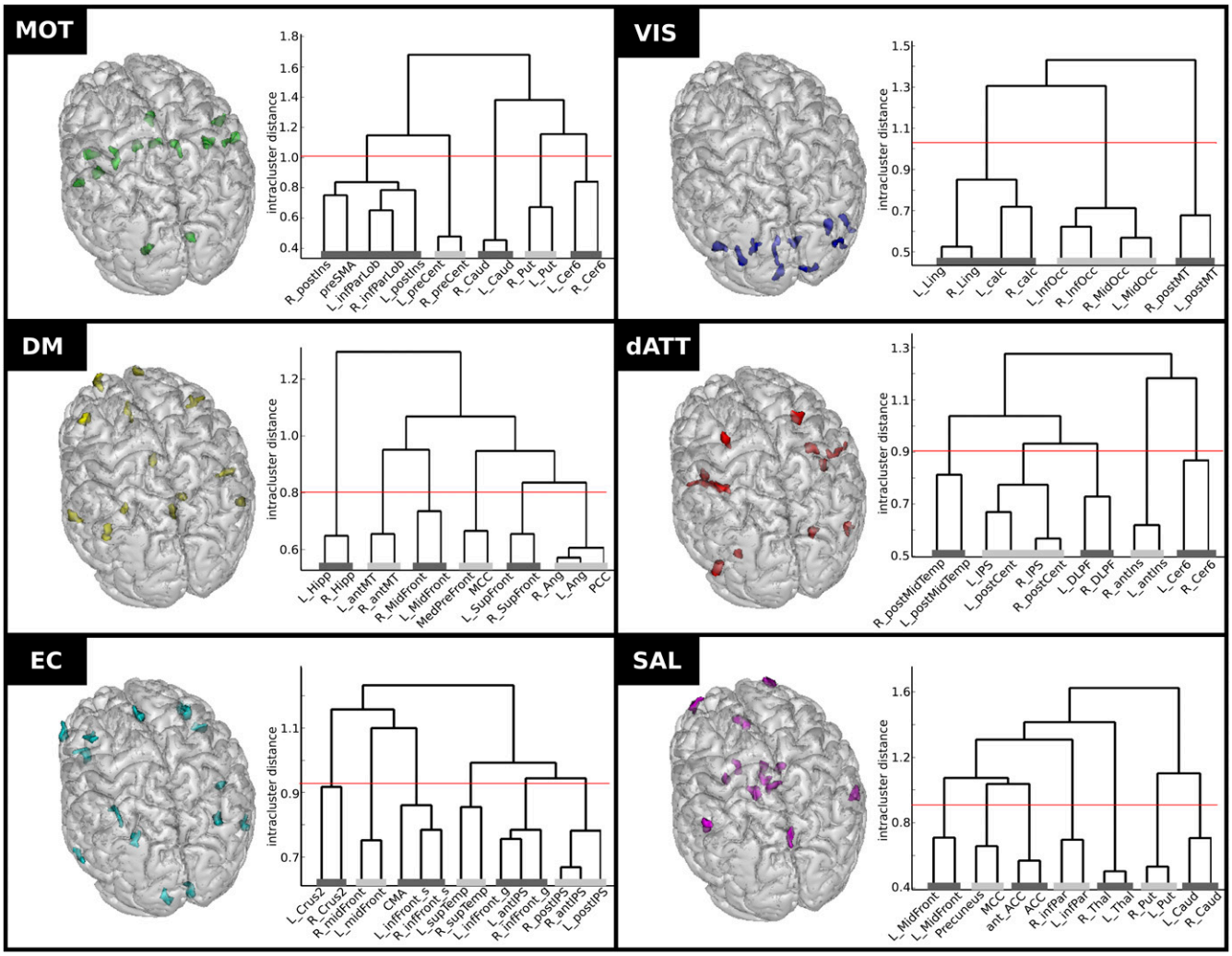


**Fig. S2.** The color-coded assemblies of the default mode network, projected in tridimensional brain space (*Left* in each box) and the assemblies defined from the thresholded similarity trees for each network (*Right* in each box). Neuroanatomy-based segregation is shown.

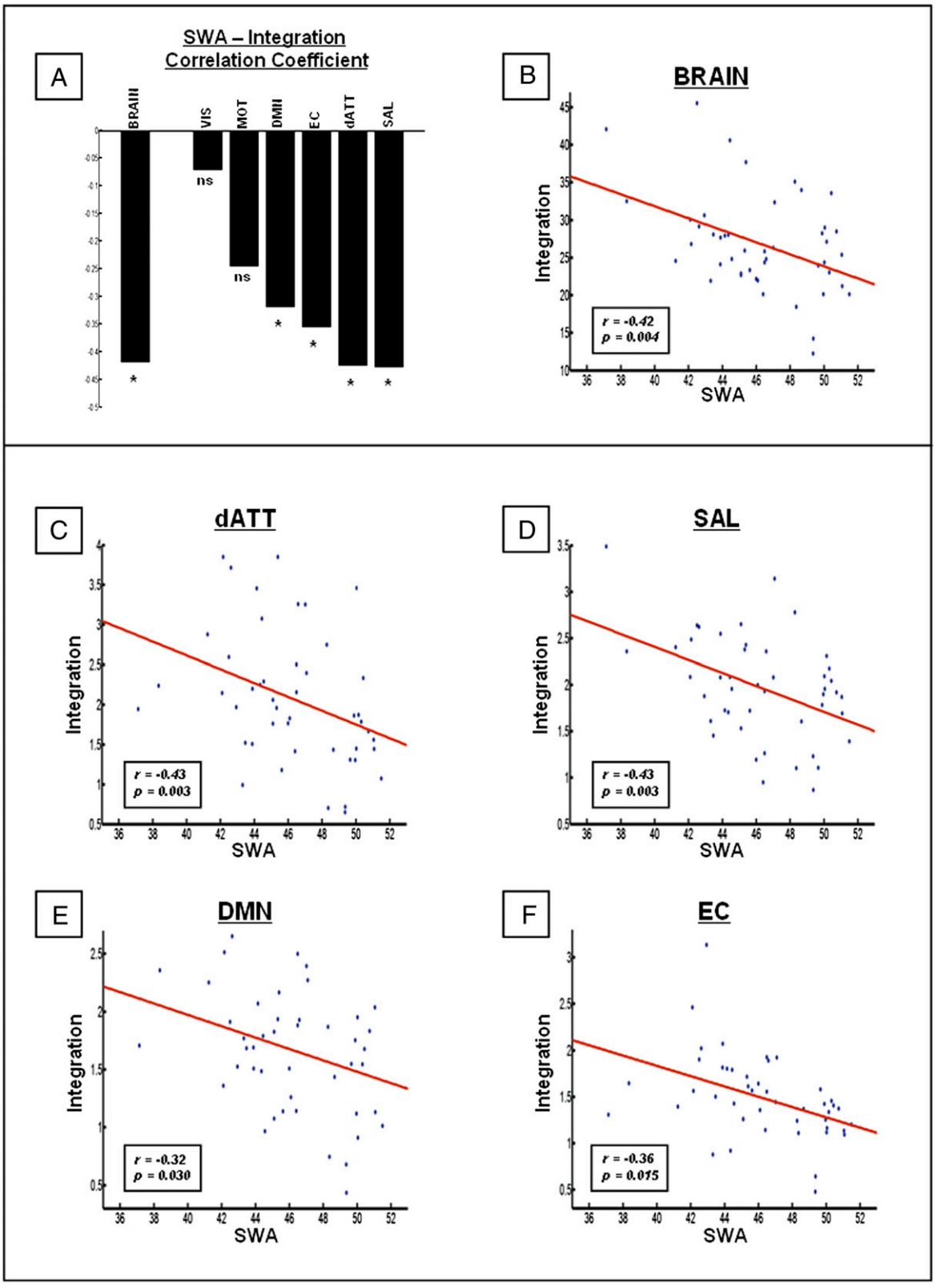


**Fig. S3.** (*A–F*) Slow-wave activity decreases total brain integration. *Significant at $P < 0.05$; ns, not significant.

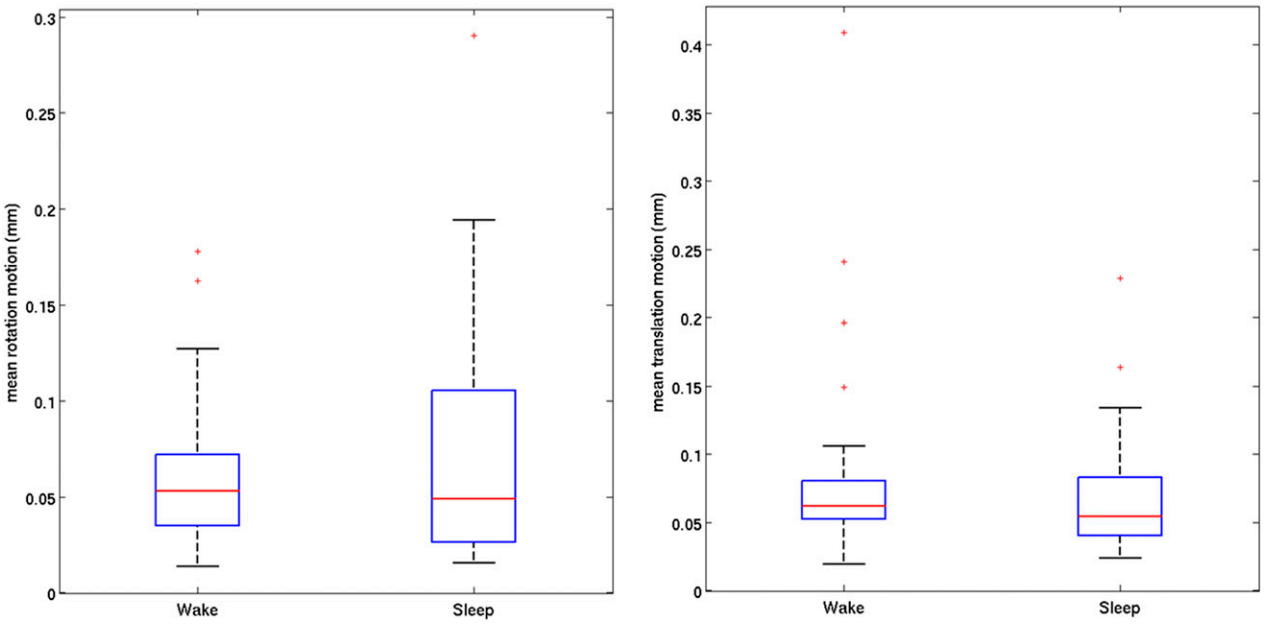


**Fig. S4.** Rotation and translation movement amplitude during wakefulness and NREM sleep fMRI acquisition sessions.

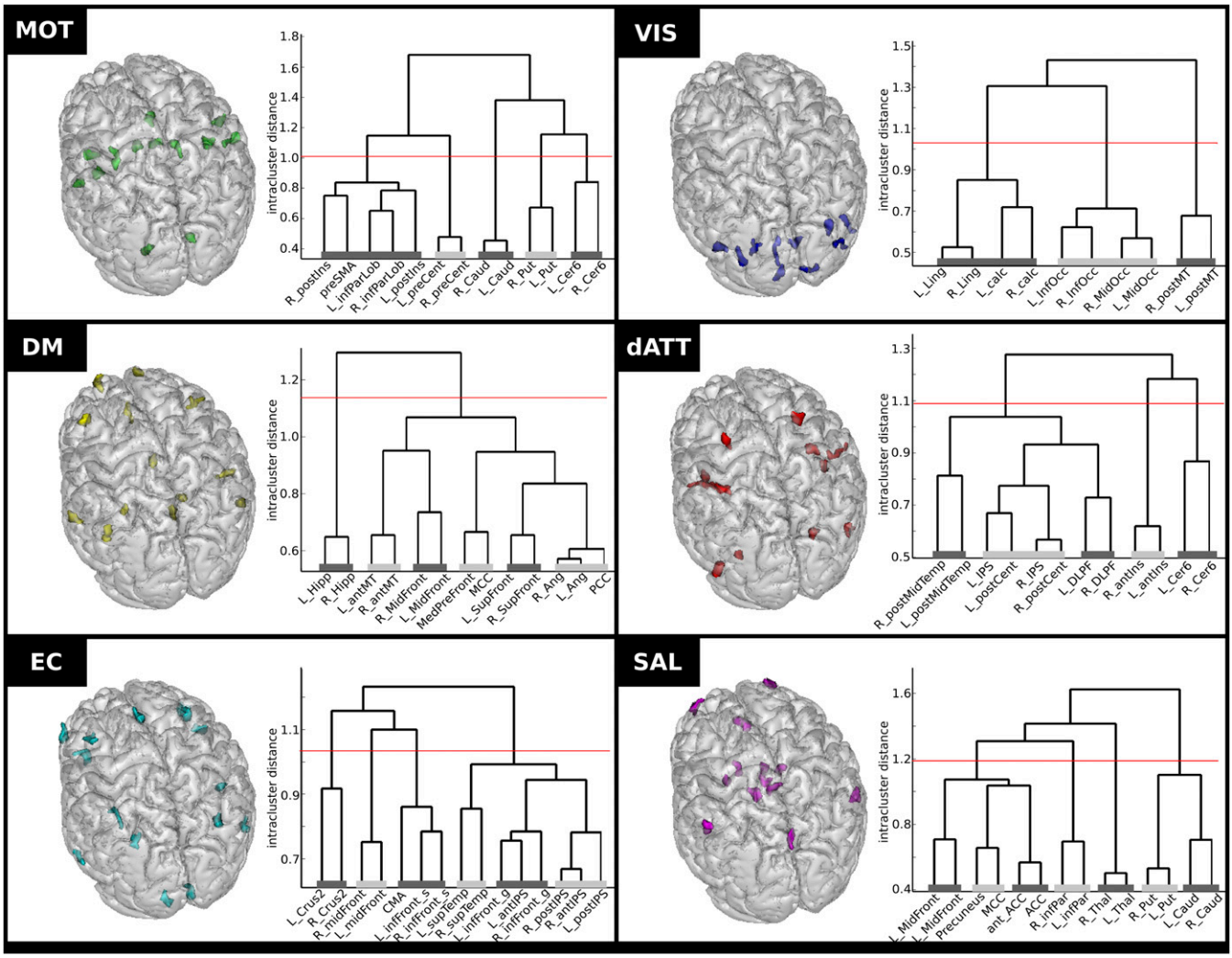


**Fig. S5.** The color-coded assemblies of the default mode network, projected in tridimensional brain space (*Left* in each box) and the assemblies defined from the thresholded similarity trees for each network (*Right* in each box). Homogenous assembly distribution threshold is shown.

**Table S1. Talairach coordinates and labels of regions of interest selected within each network**

| Region name | Abbrev. | *x* | *y* | *z* |
|---|---|---|---|---|
| Network MOT | | | | |
| Presupplementary motor area | PreSMA | 0 | 2 | 51 |
| Left precentral gyrus | L_preCent | −50 | −9 | 40 |
| Right precentral gyrus | R_preCent | 47 | −7 | 38 |
| Left anterior inferior parietal lobule | L_infParLob | −61 | −14 | 14 |
| Right anterior inferior parietal lobule | R_infParLob | 57 | −14 | 14 |
| Left posterior insula | L_postIns | −47 | −4 | −1 |
| Right posterior insula | R_postIns | 42 | −11 | 15 |
| Left caudate nucleus | L_Caud | −6 | 1 | 10 |
| Right caudate nucleus | R_Caud | 6 | 3 | 10 |
| Left putamen | L_put | −23 | −2 | 2 |
| Right putamen | R_put | 22 | 3 | 0 |
| Left cerebellum, VI | L_Cer6 | −16 | −60 | −22 |
| Right cerebellum, VI | R_Cer6 | 18 | −61 | −19 |
| Network DM | | | | |
| Left middle frontal gyrus | L_MidFront | −40 | 17 | 44 |
| Right middle frontal gyrus | R_MidFront | 42 | 27 | 41 |
| Left polar superior frontal gyrus | L_SupFront | −16 | 65 | 13 |
| Right polar superior frontal gyrus | R_SupFront | 14 | 66 | 11 |
| Pregenual medial prefrontal cortex | MedPreFront | −3 | 45 | −5 |
| Left angular gyrus | L_Ang | −49 | −62 | 36 |
| Right angular gyrus | R_Ang | 51 | −56 | 33 |
| Posterior cingulate cortex | PCC | 0 | −53 | 32 |
| Middle cingulate cortex | MCC | 2 | −14 | 36 |
| Left anterior middle temporal gyrus | L_antMT | −59 | −14 | −14 |
| Right anterior middle temporal gyrus | R_antMT | 59 | −16 | −14 |
| Left hippocampus | L_Hipp | −22 | −21 | −13 |
| Right hippocampus | R_Hipp | 22 | −21 | −17 |
| Network EC | | | | |
| Left inferior frontal sulcus | L_infFront_s | −44 | 12 | 29 |
| Right inferior frontal sulcus | R_infFront_s | 44 | 15 | 30 |
| Left middle frontal gyrus | L_midFront | −33 | 15 | 54 |
| Right middle frontal gyrus | R_midFront | 40 | 16 | 52 |
| Cingulate motor area | CMA | 0 | 27 | 42 |
| Left inferior frontal gyrus | L_infFront_g | −44 | 45 | −3 |
| Right inferior frontal gyrus | R_infFront_g | 46 | 50 | −2 |
| Left posterior intraparietal sulcus | L_postIPS | −29 | −68 | 47 |
| Right posterior intraparietal sulcus | R_postIPS | 33 | −65 | 47 |
| Left anterior intraparietal sulcus | L_antIPS | −39 | −43 | 48 |
| Right anterior intraparietal sulcus | R_antIPS | 41 | −45 | 50 |
| Left superior temporal sulcus | L_supTemp | −60 | −51 | −9 |
| Right superior temporal sulcus | R_supTemp | 65 | −43 | −3 |
| Left cerebellum, Crus2 | L_Crus2 | −9 | −80 | −25 |
| Right cerebellum, Crus2 | R_Crus2 | 10 | −83 | −23 |
| Network VIS | | | | |
| Left calcarine fissure | L_calc | −6 | −97 | 5 |
| Right calcarine fissure | R_calc | 13 | −80 | −4 |
| Left lingual gyrus | L_Ling | −4 | −73 | 2 |
| Right lingual gyrus | R_Ling | 9 | −73 | −3 |
| Left middle occipital gyrus | L_MidOcc | −26 | −81 | 30 |
| Right middle occipital gyrus | R_MidOcc | 31 | −80 | 28 |
| Left inferior occipital gyrus | L_InfOcc | −32 | −90 | 16 |
| Right inferior occipital gyrus | R_InfOcc | 40 | −78 | 15 |
| Left posterior middle temporal sulcus | L_postMT | −45 | −73 | 5 |
| Right posterior middle temporal sulcus | R_postMT | 51 | −64 | 7 |
| Network dATT | | | | |
| Left dorsolateral prefrontal cortex | L_DLPF | −27 | 0 | 61 |
| Right dorsolateral prefrontal cortex | R_DLPF | 29 | −3 | 62 |
| Left postcentral gyrus | L_postCent | −51 | −23 | 39 |
| Right postcentral gyrus | R_postCent | 50 | −21 | 41 |
| Left intraparietal sulcus | L_IPS | −34 | −38 | 55 |
| Right intraparietal sulcus | R_IPS | 41 | −32 | 52 |
| Left posterior middle temporal gyrus | L_postMidTemp | −50 | −62 | −4 |

**Table S1. Cont.**

| Region name | Abbrev. | *x* | *y* | *z* |
|---|---|---|---|---|
| Right posterior middle temporal gyrus | R_postMidTemp | 51 | −64 | −4 |
| Left anterior insula | L_antIns | −41 | −2 | 8 |
| Right anterior insula | R_antIns | 40 | 0 | 5 |
| Left cerebellum, VI | L_Cer6 | −29 | −47 | −25 |
| Right cerebellum, VI | R_Cer6 | 29 | −49 | −23 |
| Network SAL | | | | |
| Left polar middle frontal gyrus | L_midFront | −27 | 57 | 25 |
| Right polar middle frontal gyrus | R_midFront | 29 | 56 | 22 |
| Precuneus | Precuneus | 2 | −71 | 49 |
| Left inferior parietal lobule | L_infPar | −56 | −44 | 44 |
| Right inferior parietal lobule | R_infPar | 56 | −49 | 39 |
| Anterior cingulate cortex | ant_ACC | 0 | 41 | 13 |
| Anterior cingulate cortex | ACC | 0 | 27 | 32 |
| Middle cingulate cortex | MCC | 0 | −14 | 30 |
| Left caudate nucleus | L_Caud | −7 | 7 | 1 |
| Right caudate nucleus | R_Caud | 12 | 11 | 5 |
| Left putamen | L_put | −21 | 7 | 8 |
| Right putamen | R_put | 19 | 10 | 7 |
| Left thalamus | L_Thal | −8 | −13 | 9 |
| Right thalamus | R_Thal | 6 | −12 | 7 |

Abbrev., abbreviation.

**Table S2. Individual FCR results**

| | FCR variations prob > 0.95 | | | | | | | | | | | | | |
|---|---|---|---|---|---|---|---|---|---|---|---|---|---|---|
| Networks | Sub 1 | Sub 2 | Sub 3 | Sub 4 | Sub 5 | Sub 6 | Sub 7 | Sub 8 | Sub 9 | Sub 10 | Sub 11 | Sub 12 | Sub 13 | Num (+) |
| Brain | (+) | (−) | (+) | (−) | (=) | (+) | (=) | (+) | (=) | (+) | (+) | (+) | (+) | 8 |
| MOT | (+) | (+) | (+) | (−) | (+) | (+) | (+) | (+) | (+) | (+) | (+) | (+) | (+) | 12 |
| VIS | (+) | (+) | (+) | (+) | (−) | (+) | (+) | (+) | (+) | (+) | (+) | (+) | (+) | 12 |
| DM | (+) | (+) | (+) | (−) | (−) | (+) | (+) | (+) | (+) | (+) | (+) | (+) | (+) | 11 |
| dATT | (+) | (+) | (+) | (+) | (+) | (+) | (+) | (+) | (+) | (+) | (+) | (+) | (+) | 13 |
| EC | (+) | (+) | (+) | (+) | (+) | (+) | (+) | (+) | (=) | (+) | (+) | (+) | (+) | 12 |
| SAL | (+) | (+) | (+) | (+) | (+) | (+) | (+) | (+) | (+) | (+) | (+) | (+) | (+) | 13 |
| Num (+) | 7 | 6 | 7 | 4 | 4 | 7 | 6 | 7 | 5 | 7 | 7 | 7 | 7 | |

(+) denotes a probability of increase of FCR in NREM sleep compared with wakefulness >0.95. Sub, subject.

**Table S3. Sleep parameters**

| Parameter | Mean (SD) |
|---|---|
| Total sleep time, min | 71.10 (26.91) |
| N2 sleep latency | 10.52 (8.80) |
| N2 sleep duration, min | 44.79 (23.95) |
| N3 sleep duration, min | 26.29 (15.92) |
| REM sleep duration, min | 0 (0) |
| Sleep efficiency, % | 0.70 (0.18) |

N2, stage 2; N3, stage 3.

**Table S4. Functional clustering ratios (FCR) computed within whole brain and within each network during wakefulness and NREM sleep after regression of movement parameters during the computation of regions-of-interest time series**

| | Wakefulness | | NREM sleep–wakefulness | Sleep | |
|---|---|---|---|---|---|
| FCR = $I_{ws}/I_{bs}$ | Mean | SD | Variations prob > 0.95 | Mean | SD |
| Brain level vs. networks | | | | | |
| Brain | 1.53 | 0.03 | (+) | 1.70 | 0.03 |
| System level vs. assemblies | | | | | |
| MOT | 4.87 | 0.29 | (+) | 6.26 | 0.37 |
| VIS | 3.02 | 0.28 | (+) | 6.70 | 0.42 |
| DM | 0.96 | 0.05 | (+) | 1.28 | 0.06 |
| dATT | 1.32 | 0.10 | (+) | 1.99 | 0.09 |
| EC | 0.54 | 0.04 | (+) | 1.02 | 0.05 |
| SAL | 1.39 | 0.07 | (+) | 3.77 | 0.18 |

The central column in Tables S6–S9 indicates the variations with a probability >0.95.

**Table S5. Total integration values computed within whole brain and within each network during wakefulness and NREM sleep after regression of movement parameters during the computation of regions-of-interest time series**

| | Wakefulness | | NREM sleep–wakefulness | Sleep | |
|---|---|---|---|---|---|
| $I_{tot}$ | Mean | SD | Variations prob > 0.95 | Mean | SD |
| Brain level vs. networks | | | | | |
| Brain | 5.40 | 0.07 | (+) | 6.15 | 0.07 |
| System level vs. assemblies | | | | | |
| MOT | 0.83 | 0.02 | (–) | 0.73 | 0.02 |
| VIS | 0.31 | 0.02 | (+) | 0.68 | 0.02 |
| DM | 0.56 | 0.02 | (=) | 0.55 | 0.02 |
| dATT | 0.32 | 0.02 | (+) | 0.64 | 0.02 |
| EC | 0.40 | 0.02 | (+) | 0.56 | 0.02 |
| SAL | 0.84 | 0.02 | (–) | 0.70 | 0.02 |

**Table S6. Within-subsystems integration values computed for whole brain and for each network during wakefulness and NREM sleep after regression of movement parameters during the computation of regions-of-interest time series**

| | Wakefulness | | NREM sleep–wakefulness | Sleep | |
|---|---|---|---|---|---|
| $I_{ws}$ | Mean | SD | Variations prob > 0.95 | Mean | SD |
| Brain level vs. networks | | | | | |
| Brain | 3.27 | 0.06 | (+) | 3.98 | 0.05 |
| System level vs. assemblies | | | | | |
| MOT | 0.69 | 0.02 | (–) | 0.63 | 0.02 |
| VIS | 0.23 | 0.01 | (+) | 0.59 | 0.02 |
| DM | 0.27 | 0.01 | (+) | 0.31 | 0.01 |
| dATT | 0.18 | 0.01 | (+) | 0.43 | 0.01 |
| EC | 0.14 | 0.01 | (+) | 0.28 | 0.01 |
| SAL | 0.49 | 0.02 | (+) | 0.56 | 0.01 |

**Table S7. Between-subsystems integration values computed for whole brain and for each network during wakefulness and NREM sleep after regression of movement parameters during the computation of regions-of-interest time series**

| Wakefulness | | | NREM sleep–wakefulness | Sleep | |
|---|---|---|---|---|---|
| $I_{bs}$ | Mean | SD | Variations prob > 0.95 | Mean | SD |
| Brain level vs. networks | | | | | |
| Brain | 2.18 | 0.04 | (+) | 2.39 | 0.03 |
| System level vs. assemblies | | | | | |
| MOT | 0.14 | 0.01 | (–) | 0.10 | 0.01 |
| VIS | 0.08 | 0.01 | (=) | 0.09 | 0.01 |
| DM | 0.29 | 0.01 | (–) | 0.24 | 0.01 |
| dATT | 0.14 | 0.01 | (+) | 0.22 | 0.01 |
| EC | 0.26 | 0.01 | (=) | 0.28 | 0.01 |
| SAL | 0.35 | 0.02 | (–) | 0.15 | 0.01 |

**Table S8. Functional clustering ratios (FCR) computed within whole brain and within each network during wakefulness (W) and NREM sleep, using the network partitions defined from the homogenous assembly distribution method**

| Wakefulness | | | NREM sleep–wakefulness | Sleep | |
|---|---|---|---|---|---|
| FCR = $I_{ws}/I_{bs}$ | Mean | SD | Variations prob > 0.95 | Mean | SD |
| Brain level vs. networks | | | | | |
| Brain | 1.50 | 0.03 | (+) | 1.70 | 0.03 |
| Network level vs. assemblies | | | | | |
| MOT | 4.72 | 0.30 | (+) | 5.95 | 0.37 |
| VIS | 2.92 | 0.27 | (+) | 6.24 | 0.37 |
| DM | 15.48 | 2.03 | (+) | 40.88 | 6.70 |
| dATT | 4.37 | 0.47 | (+) | 8.98 | 0.70 |
| EC | 1.52 | 0.12 | (+) | 3.54 | 0.22 |
| SAL | 3.80 | 0.23 | (+) | 14.44 | 1.36 |

The central column indicates the variations with a probability >0.95.

**Table S9. Functional clustering ratios (FCR) for MOT, VIS, and SAL networks using the system–subsystems organization defined from NREM sleep data**

| Wakefulness | | | NREM sleep–wakefulness | Sleep | |
|---|---|---|---|---|---|
| FCR = $I_{ws}/I_{bs}$ | Mean | SD | Variations prob > 0.95 | Mean | SD |
| Network level vs. assemblies | | | | | |
| MOT | 4.48 | 0.36 | (+) | 13.00 | 0.92 |
| VIS | 4.23 | 0.38 | (+) | 5.50 | 0.28 |
| SAL | 1.51 | 0.08 | (+) | 2.84 | 0.13 |

The central column indicates the variations with a probability >0.95.

**Table S10. Functional clustering ratios (FCR) using the FCR values for each system of interest using subsystems defined from wakefulness data for hierarchical clustering**

| Wakefulness | | | NREM sleep–wakefulness | Sleep | |
|---|---|---|---|---|---|
| FCR = $I_{ws}/I_{bs}$ | Mean | SD | Variations prob > 0.95 | Mean | SD |
| Brain level vs. networks | | | | | |
| Brain | 1.50 | 0.03 | (+) | 1.70 | 0.03 |
| Network level vs. assemblies | | | | | |
| MOT | 13.23 | 1.28 | (+) | 19.78 | 2.21 |
| VIS | 2.92 | 0.27 | (+) | 6.24 | 0.37 |
| DM | 0.93 | 0.06 | (+) | 1.24 | 0.06 |
| dATT | 2.68 | 0.21 | (+) | 3.97 | 0.24 |
| EC | 0.55 | 0.04 | (+) | 0.68 | 0.03 |
| SAL | 3.79 | 0.23 | (+) | 13.72 | 1.24 |

The central column indicates the variations with a probability >0.95.